Journal of Magnetic Resonance **137,** 144–153 (1999)
Article ID jmre.1998.1642, available online at http://www.idealibrary.com on IDEAL®

Single-Shot Line Scan Imaging Using Stimulated Echoes

Jürgen Finsterbusch and Jens Frahm[1]

Biomedizinische NMR Forschungs GmbH am Max-Planck-Institut für biophysikalische Chemie, D-37070 Göttingen, Germany

Received July 23, 1998; revised October 22, 1998

A new high-speed MRI method is described for single-shot line scan imaging (LSI) based on stimulated echoes (STE). To allow for multislice imaging, the technique comprises a series of slice-selective preparation pulses (each corresponding to the first RF pulse of a STE sequence), a slab-selective refocusing pulse (second RF pulse), and multiple line-selective read pulses (third RF pulses). An alternative version employs packages of two slice-selective pulses followed by multiple line-selective read pulses. Experimental applications deal with human brain imaging on a clinical MRI system at 2.0 T. The technique offers user-selectable trade-offs between volume coverage (1–15 sections) and in-plane spatial resolution (1–5 mm linear pixel dimension) within total acquisition times of less than 500 ms. Although LSI yields a lower signal-to-noise ratio than Fourier imaging, single-shot LSI with STEs is free from resonance offset effects (e.g., magnetic field inhomogeneities and susceptibility differences) that are typical for echo-planar imaging. Moreover, the technique exhibits considerable robustness against motion and provides access to arbitrary fields-of-view, i.e., localized imaging of inner volumes without aliasing artifacts due to phase wrapping.

Key Words: **magnetic resonance imaging; high-speed imaging; single-shot imaging; line scan imaging; human brain.**

INTRODUCTION

Line scan imaging (LSI) techniques were among the first approaches to magnetic resonance imaging (MRI) (*1–5*). Image reconstruction is accomplished by multiple independent acquisitions of signals from columnar "lines" of magnetization followed by 1D Fourier transformation and a proper arrangement of the resulting line intensity projections into a 2D array.

Although LSI was rapidly abandoned during the historic development of MRI because of its inherently low efficiency in comparison to Fourier imaging (*6*), it bears some interesting features not available with Fourier methods. In particular, the absence of spatial phase-encoding eliminates corresponding motion errors and their propagation through image space. Accordingly, renewed interest in LSI is mainly motivated by the robustness against involuntary subject motions in critically sensitive applications such as diffusion-weighted MRI. Whereas current diffusion studies often employ echo-planar imaging (EPI) to overcome the motion problem, e.g., see (*7*), they introduce other image artifacts such as signal losses and geometric distortions that are caused by the unavoidable EPI sensitivity to chemical shift effects, magnetic field inhomogeneities, and susceptibility differences. A convenient principle for LSI is to define columnar strips of magnetizations by the cross-section of two slice-selective RF pulses (*4, 5*). In order to avoid saturation of subsequent line magnetization, both the excitation and refocusing plane may be rotated out of the desired image plane (*8*). Diffusion-weighted modifications achieved measuring times of about 20–30 s per section (*9, 10*).

The first single-shot LSI sequence (*11*) used stimulated echo (STE) signals that were generated by two identical slice-selective RF pulses and a series of spatially shifted "third" RF pulses perpendicular to the excited image plane. A more recent spin-echo (SE) analogue refocuses a series of slice-selective RF excitation pulses with a single perpendicular slice-selective 180° RF pulse (*12*). These single-shot LSI techniques are single-slice sequences because the various line excitations lead to spatial saturation of magnetizations outside the image plane and therefore preclude rapidly repeated measurements of adjacent sections. To overcome this limitation and to allow for high-speed volume coverage, the present work proposes the adaptation of multiple-echo encoding elements (*12*) for the development of single-shot multi-slice LSI sequences based on STE signals. Preliminary applications deal with imaging of the human brain with measuring times of less than 500 ms.

METHODS

Single-Shot Multislice LSI Sequences

Figure 1 shows two basic pulse sequences for single-shot multislice LSI using STEs. The examples refer to the acquisition of 3 sections. For sake of simplicity spoiler gradients are omitted. The denotation of the logical gradient directions is adapted to LSI as 'Line' replaces 'Phase' for Fourier imaging. Its orientation is along the direction of line progression.

When using partially slab-selective preparation as shown in Fig. 1a, the sections are sequentially excited by a series of slice-selective RF pulses. The corresponding slice-selection gradients are rephased by alternating the sign of consecutive gradient pulses as well as by a final gradient lobe after the last RF pulse of the excitation part. A cumulative predephasing readout gradient is applied after each of the RF excitation pulses. This ensures proper rephasing of the STE signals that

[1] To whom correspondence should be addressed. E-mail: jfrahm@gwdg.de.

1090-7807/99 $30.00

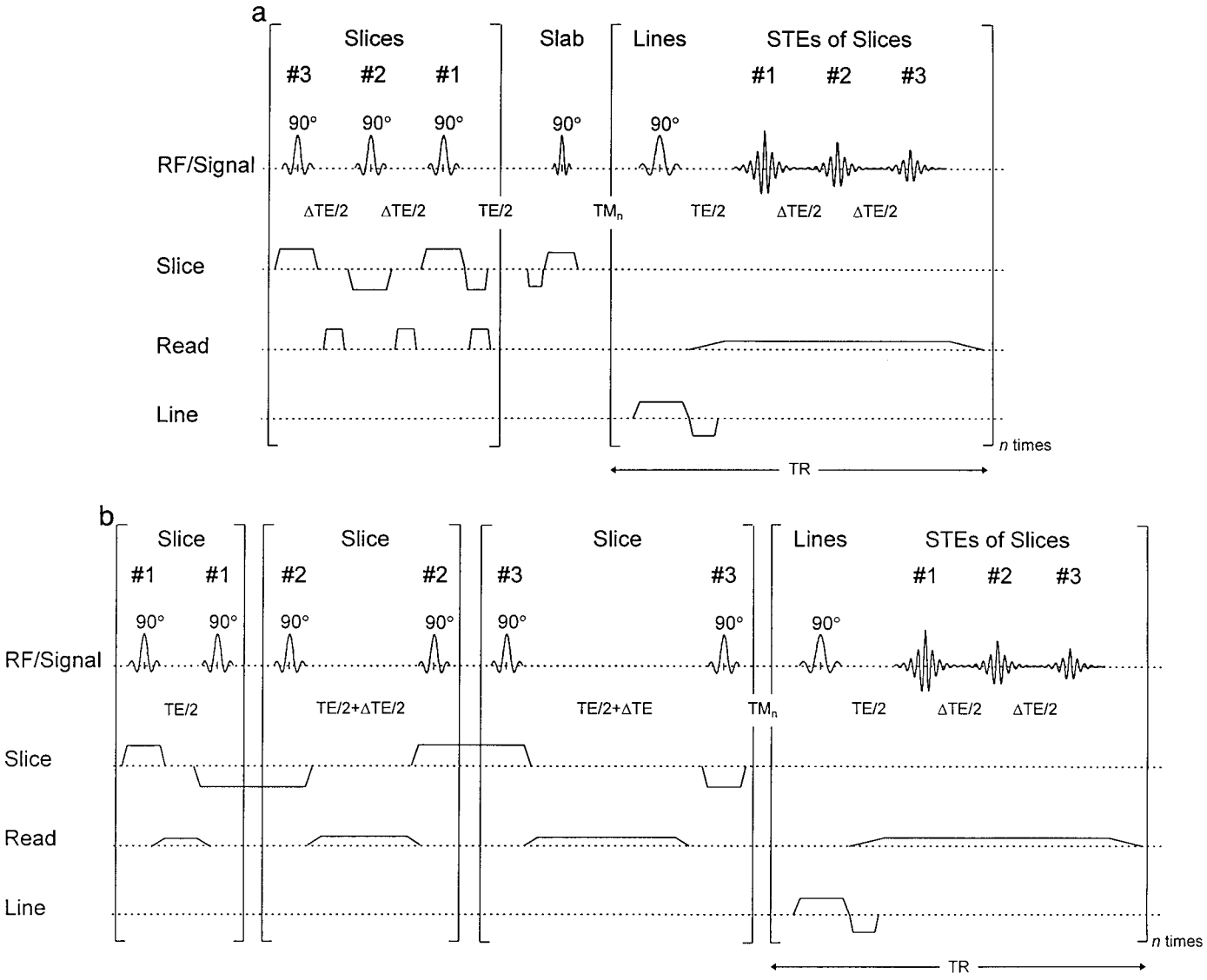

FIG. 1. Single-shot multislice line scan imaging using stimulated echoes (for three sections). (a) Basic sequence with slice-selective excitation pulses (first bracket) and a single slab-selective refocusing pulse, and (b) alternative version with two slice-selective preparation pulses per section (first three brackets). In both cases the lines for a full image are defined by repetitive applications (n times) of a spatially shifted line-selective read pulse (last bracket).

are temporarily separated during data acquisition in accordance with the echo time offset $\Delta TE/2$ in between slice-selective RF pulses. Slice-selective preparation is terminated by a slab-selective (or even nonselective) RF pulse which simultaneously realigns the magnetizations of all sections along the longitudinal direction. The final step involves a slice-selective readout RF pulse in line direction, i.e., perpendicular to the image plane, that generates STEs from the columnar intersections with the initially prepared sections. Because of their different timings and accumulated phases in readout direction, the magnetizations of the individual slice-selective STEs refocus at different echo times.

In the alternative sequence shown in Fig. 1b, sequential packages of two slice-selective RF pulses excite and realign pertinent magnetizations for all sections individually. Complete rephasing is achieved by inverting the sign of the second slice-selective gradient relative to the first one. The preparative step is repeated for all sections with increasing echo times and predephasing readout gradients to achieve echo time offsets for the final STE signals.

The data of each STE are Fourier transformed and stored as a line of 1D intensities in a 2D image array. Full line scan images are obtained by multiple repetitions of the final line-selective readout RF pulse applied to spatially shifted planes. Spoiler gradients must be introduced to the basic sequences of Fig. 1 to ensure sufficient suppression of unwanted signals. This is especially important for the line-selective generation of the STEs as their intensities compete with the unwanted FID

TABLE 1
Parameters for Single-Shot Line Scan Imaging Using Stimulated Echoes

Number of sections[a]	1	1	3	5	7	15
Sequence version	Slab-selective	Slab-selective	Slab-selective	Slab-selective	Slice-selective	Slice-selective
Imaging time	457 ms	368 ms	443 ms	484 ms	386 ms	371 ms
per section	—	—	148 ms	97 ms	55 ms	25 ms
Number of lines	40	40	40	40	32	24
FOV/mm^2	256 × 80	384 × 120	384 × 120	384 × 120	240 × 120	320 × 120
Pixel/mm^2	1.0 × 2.0	1.5 × 3.0	1.5 × 3.0	3.0 × 3.0	3.75 × 3.75	5.0 × 5.0
Display[b]	1.0 × 1.0	1.5 × 1.5	1.5 × 1.5	3.0 × 3.0	1.88 × 1.88	2.5 × 2.5
SNR[c]	17	41	23	42	50	51
First TE	11.08 ms	8.90 ms	5.70 ms	4.94 ms	4.50 ms	3.96 ms
ΔTE	—	—	4.88 ms	3.34 ms	2.06 ms	1.04 ms
Acq/echo	8.320 ms	5.632 ms	2.432 ms	1.664 ms	1.024 ms	0.512 ms
TR/line	11.03 ms	8.87 ms	10.65 ms	11.64 ms	10.46 ms	11.04 ms

[a] All sections had a thickness of 5 mm, slice gaps were 1.25 mm.
[b] To facilitate direct comparisons, all images displayed in Figs. 2–6 are scaled to a FOV of 200 mm.
[c] For the central section of a water phantom.

from a complete slice perpendicular to the image plane. Furthermore, sufficient dephasing is required to decouple the acquisition of subsequent STE signals.

MRI Studies of Human Brain

All studies were conducted at 2.0 T using a whole-body MRI system (Magnetom Vision, Siemens, Erlangen, Germany) with 25 mT m^{-1} gradients (maximum slew rate 40 mT m^{-1} ms^{-1}). Images were obtained with the standard circularly polarized head coil. Conventional data processing for Fourier imaging was adapted to LSI requirements. In particular, filtering and Fourier transformation were discarded along the direction of the moving lines, i.e., in the direction of the usual 2D phase-encoding gradient. If applied, postacquisition image processing involved a linear interpolation of intensities from neighboring lines.

Measurements were carried out on phantoms and healthy young subjects. Written informed consent was obtained in all cases before the examinations. Transverse single-shot multislice LSI of the brain was performed by exciting sections from head to feet and lines from right to left (or reverse). Anatomical, fast scan, and high-speed images were obtained with use of fast spin echo sequences (FSE, TR/TE = 2625/98 ms, 5 echoes per TR, 0.95 × 0.95 mm^2 pixel resolution, 15 sections, measuring time 2 min 16 s), low flip angle gradient-echo sequences (FLASH, TR/TE = 45/4 ms, 1.5 × 3.0 mm^2, measuring time 6.3 s), and single-shot blipped spin-echo EPI (SE-EPI, TE = 70 ms, 1.88 × 1.88 mm^2, measuring time 168 ms).

RESULTS AND DISCUSSION

Table 1 summarizes a variety of single-shot LSI sequences that have been experimentally realized to analyze achievable trade-offs between volume coverage (1–15 sections), in-plane resolution (1–5 mm linear pixel dimension), and signal-to-noise ratio (SNR). Moreover, different implementations served to facilitate comparisons with conventional, fast scan, and high-speed imaging sequences. In all cases the total imaging time has been kept below 500 ms.

In general, the choice of a particular LSI sequence depends on the desired bandwidth (i.e., SNR), the number of STEs per echo train (i.e., the number of sections), the number of lines (i.e., the FOV and resolution), the RF pulse duration, and the slew rate of the gradient system. For example, if high spatial resolution prolongs the acquisition period, then preference may be given to the slab-selective LSI version shown in Fig. 1a because it leads to a shorter overall preparation period. On the other hand, coarse resolution in the direction of the readout gradient renders true slice-selective preparation advantageous as shown in Fig. 1b. In this case, shorter acquisition periods decrease the echo train length which allows an increase in the number of sections.

Whereas Fourier imaging employs spatial phase encoding, LSI achieves resolution along one image dimension by slice selection which, for identical in-plane resolution, requires stronger gradients. Nevertheless, as far as hardware requirements are concerned, the availability of a fast gradient system is not as important for single-shot LSI as for EPI. This particularly applies to LSI with slice-selective preparation (Fig. 1b) because gradient ramp times and amplitudes only affect the first echo time TE (and thereby TR), but not ΔTE and the length of the echo train. Weaker gradients are mainly at the expense of the number of slices and lines or of the measurement time and inherent signal decay (see below). For instance, the use of 15 mT m^{-1} gradients with 1 ms rise times simply prolongs the imaging time for a LSI version with 7 sections from 386 ms (see Table 1) to 473 ms. Pertinent sequences have also been experimentally verified (data not shown).

Basic Properties of Single-Shot LSI

The image properties of a single-shot LSI measurement are demonstrated in Fig. 2 in comparison to conventional FSE imaging and high-speed SE-EPI, respectively. The most prom-

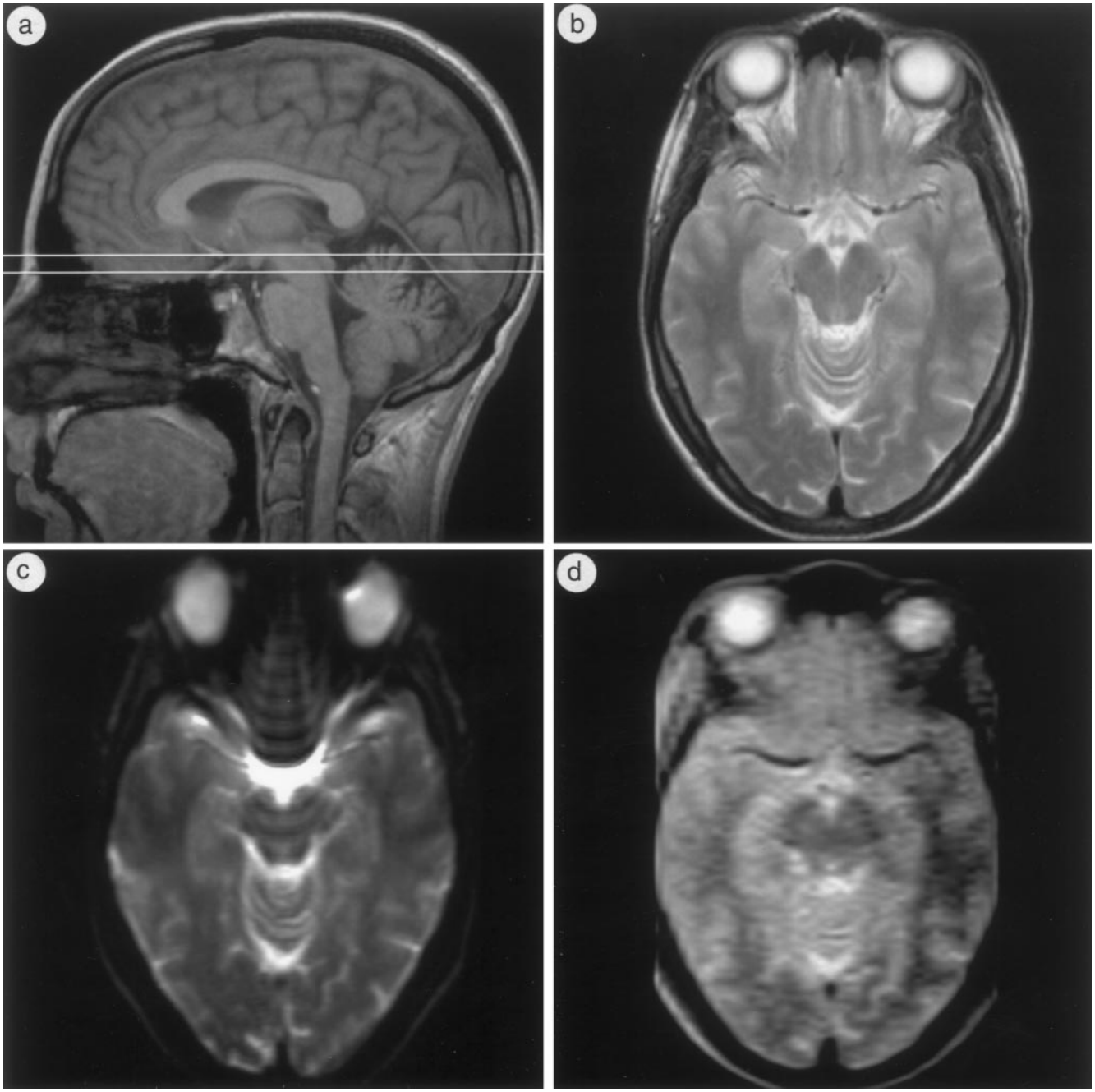

FIG. 2. Single-shot line scan imaging of the brain of a healthy young adult. (a) Localizer FLASH image (1.0×1.0 mm^2), (b) FSE image of the selected section, (c) SE-EPI (1.88×1.88 mm^2, 168 ms), and (d) single-slice line scan image (1.5×3.0 mm^2, 368 ms, for other parameters see Table 1).

inent observation is the absence of any susceptibility-induced signal losses and geometric image distortions in the line scan image shown in Fig. 2d. Whereas EPI suffers severe artifacts in critical regions such as the lower part of the brain close to major air cavities, LSI based on STEs completely avoids problems due to resonance offsets by using RF refocused echoes rather than gradient echoes.

The basic contrast of single-shot line scan images is spin density as all spins are excited only once without a history of saturation. However, strong additional contributions stem from intrinsic signal attenuations due to T1 relaxation and diffusion that occur during sequence progression. These intensity weightings are caused by an increase of the effective middle interval TM with increasing line number. The most prominent consequence is an intensity decrease that follows the history of line acquisitions within a single-shot image. Thus, “later” lines with a larger effective TM enhance the signal attenuation due to T1 and also emphasize diffusion in between the dephasing

and rephasing readout gradient lobes in related TE/2-intervals. Corresponding changes in image intensity and gray/white matter contrast are clearly visible in Fig. 2d where image lines have been acquired consecutively from left to right. Of note, the T1 contrast in LSI behaves similar to T2 attenuation in SE MRI and should not be confused with hyperintensities of short-T1 tissues in partially saturated steady-state images with short repetition times. Here, the shorter T1 value in white matter as compared to gray matter yields T1-weighted hypointensities in Fig. 2d similar to T2-weighted gray/white matter contrast in Fig. 2b. Conversely, components with large T1 values such as the fluid in the vitreous body and cerebrospinal fluid appear bright.

Inherent contrast variations of single-shot LSI methods may be alleviated by sequence design, i.e., short timings and minimum spoilers, and user-selectable choices such as a reduced FOV, i.e., a low number of lines. In the human brain images shown here, the acquisition of typically 40 lines with a line "repetition time" TR of about 10 ms corresponds to a TM_{40} interval of about 400 ms for the last line. Corresponding relaxation weightings are also known for other high-speed MRI techniques. However, in contrast to single-shot LSI, T2* relaxation in EPI (*13*), T2 relaxation in RARE (*14*) and multislice STEAM-Burst MRI (*15*), and T1 relaxation in high-speed STEAM MRI (*16*) compromise the resolution of respective Fourier images in a more general manner by modulating the point-spread function, i.e., by differently affecting the spatially phase-encoded signals. As far as diffusion is concerned, single-shot LSI is more affected than EPI and RARE and has sensitivity similar to high-speed STEAM MRI. It is less restrictive than Burst MRI which employs cumulative gradient dephasing and rephasing periods for all echo signals.

Volume Coverage

Figure 3 shows a single-shot LSI acquisition of 15 sections covering most of the human brain as indicated in the localizer image. Again, the uniform image quality without susceptibility problems in lower brain sections is a most prominent feature. With a total imaging time of 371 ms, the measuring time per section is only 25 ms for this low-resolution scan at 5 mm linear pixel dimension. As an alternative, Fig. 4 depicts line scan images of 5 sections but at an improved pixel resolution of 3.0×3.0 mm^2 acquired in a single shot within 484 ms (corresponding to 97 ms per section).

Although T2 weighting of the STEs increases with increasing section number, the resulting image intensity variations are of little importance and barely recognizable in Figs. 3 and 4. This is because the range of echo times is only about 4–20 ms for both the 5 and 15 section sequence (see Table 1). Because of the need for additional readout gradients, diffusion attenuation is more pronounced in multislice acquisitions than in single-slice LSI. Noteworthy, the extension to multislice LSI is not at the expense of SNR despite similar or even shorter measuring times (see data for a water phantom in Table 1). The linear SNR gain due to an increased voxel size in images with lower spatial resolution easily compensates for the SNR loss due to an increased received bandwidth which is only proportional to $\sqrt{1/\text{acquisition period}}$. The used acquisition periods ranged from about 0.5 to 8 ms yielding a maximum four-fold decrease in SNR due to bandwidth effects, whereas the measured pixel size increased by a factor of 12.5.

Inner Volume Imaging

The absence of spatial phase-encoding in LSI allows for high-resolution imaging of inner volumes without aliasing artifacts due to phase wrapping. Figure 5 summarizes a series of sequentially acquired single-slice line scan images of a central 80 mm portion (40 lines) of transverse sections through the human brain at a pixel resolution of 1.0×2.0 mm^2 interpolated to 1.0×1.0 mm^2. Each image was obtained within a measuring time of 457 ms. In contrast to Fourier imaging, these images required neither phase-encoding oversampling nor spatial presaturation of outer image intensities. Moreover, it should be noted that a reduction of the FOV in line direction, i.e., a reduction of the number of lines, is without expense in SNR. This property is again different to Fourier imaging in which a reduced number of phase-encoding steps decreases the total number of RF excitations.

Motion Sensitivity

Another important feature of single-shot LSI is the extremely low sensitivity to motions of or within the object under investigation. The resulting robustness against deliberate and extensive subject motion is demonstrated in Fig. 6 comparing multislice FLASH and LSI measurements (3 sections) with single-slice EPI in the (left) absence and (right) presence of shaking head movements.

The lack of major motion artifacts in single-shot LSI benefits from both the millisecond acquisition speed for individual lines and the absence of motion-induced phase errors propagating through *k* space and image space of Fourier images. In fact, the resulting 2D image represents a sequential series of "snapshot" lines through the object at respective time points. Minor intensity variations in single-shot LSI of moving objects depend on the relative direction of movements and line excitations because a parallel propagation may lead to partial presaturation of line magnetizations. Relative to the 168 ms single-slice EPI scan in Fig. 6d, the 443 ms three-slice LSI recording in Fig. 6f could have been further improved for a single-slice acquisition yielding a more comparable measuring time of only 240 ms.

CONCLUDING REMARKS

Advantageous properties of single-shot LSI using STEs are due to (i) the lack of susceptibility-related signal losses and related geometric distortions, (ii) the capability of inner volume imaging without aliasing artifacts, and (iii) considerable motion robustness. Whereas the first property stems from the elimination of resonance offset effects by RF refocused echoes,

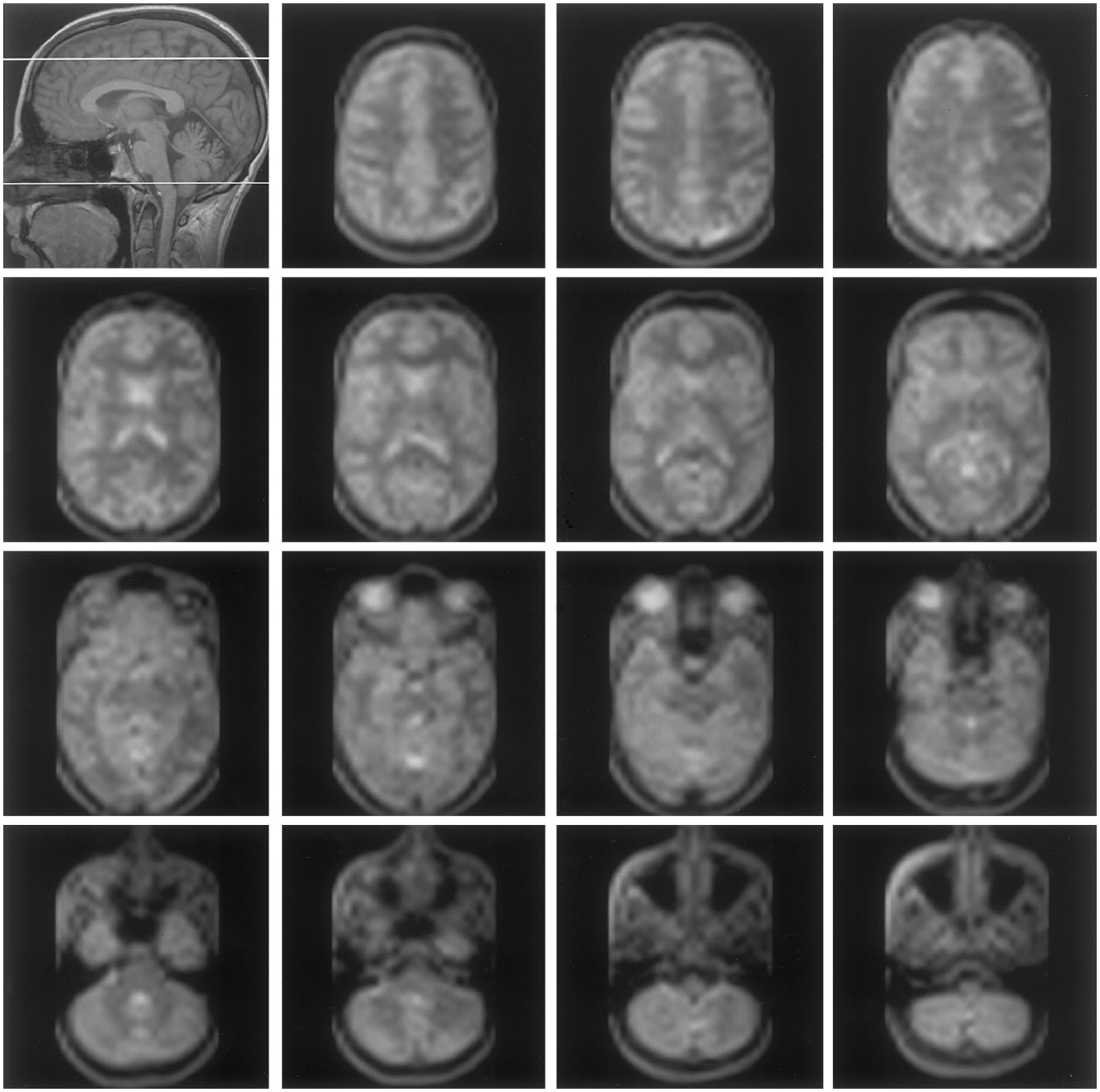

FIG. 3. Single-shot multislice line scan imaging of the brain of a healthy young adult. Localizer FLASH image (1.0×1.0 mm^2) and 15 sections with a pixel resolution of 5.0×5.0 mm^2 (interpolated to 2.5×2.5 mm^2) and a total imaging time of 371 ms (for other parameters see Table 1).

the latter two features originate from the absence of spatial phase-encoding. On the other hand, the main limitation for the present method is limited SNR because the efficiency of a line scan sequence is reduced by a factor of $\sqrt{\text{number of lines}}$ compared to 2D Fourier imaging, and because a STE recovers only half of the signal. The actually achieved SNR is lower than that for EPI, but comparable to multislice STEAM-Burst and high-speed STEAM MRI which both employ low flip angle RF pulses.

The optimum usage of single-shot LSI requires a compromise between volume coverage, spatial resolution, and SNR taking tissue-specific relaxation properties into account. Notwithstanding certain restrictions, it may find niche applications in areas such as rapid inner-volume imaging, diffusion-weighted imaging in the presence of susceptibility gradients or at high magnetic field strength, or even imaging of moving objects. Pertinent investigations are in progress.

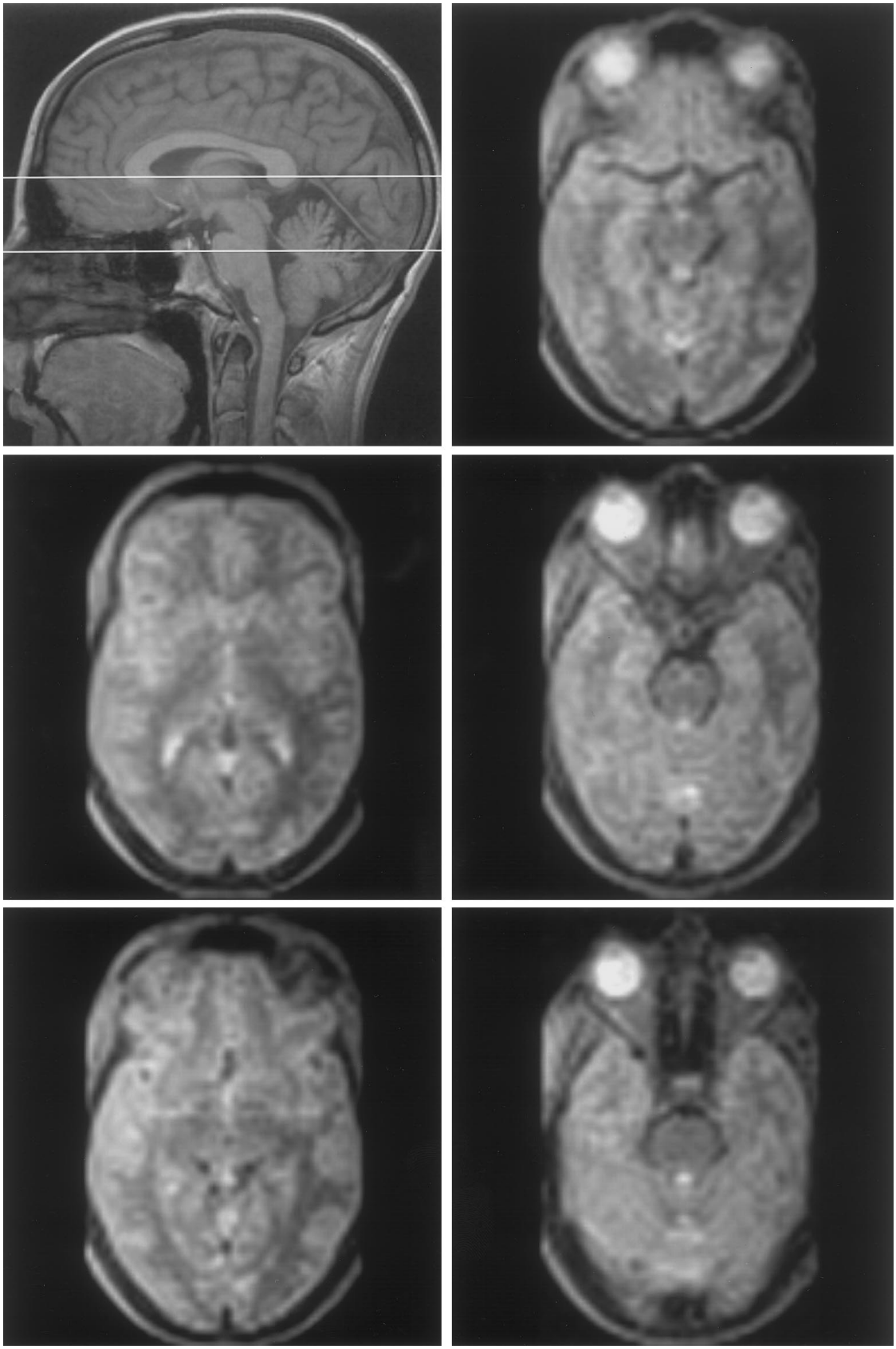

FIG. 4. Single-shot multislice line scan imaging of the brain of a healthy young adult. Localizer image (top left) and 5 sections with a pixel resolution of 3.0×3.0 mm^2 (not interpolated) and a total imaging time of 484 ms (for other parameters see Table 1).

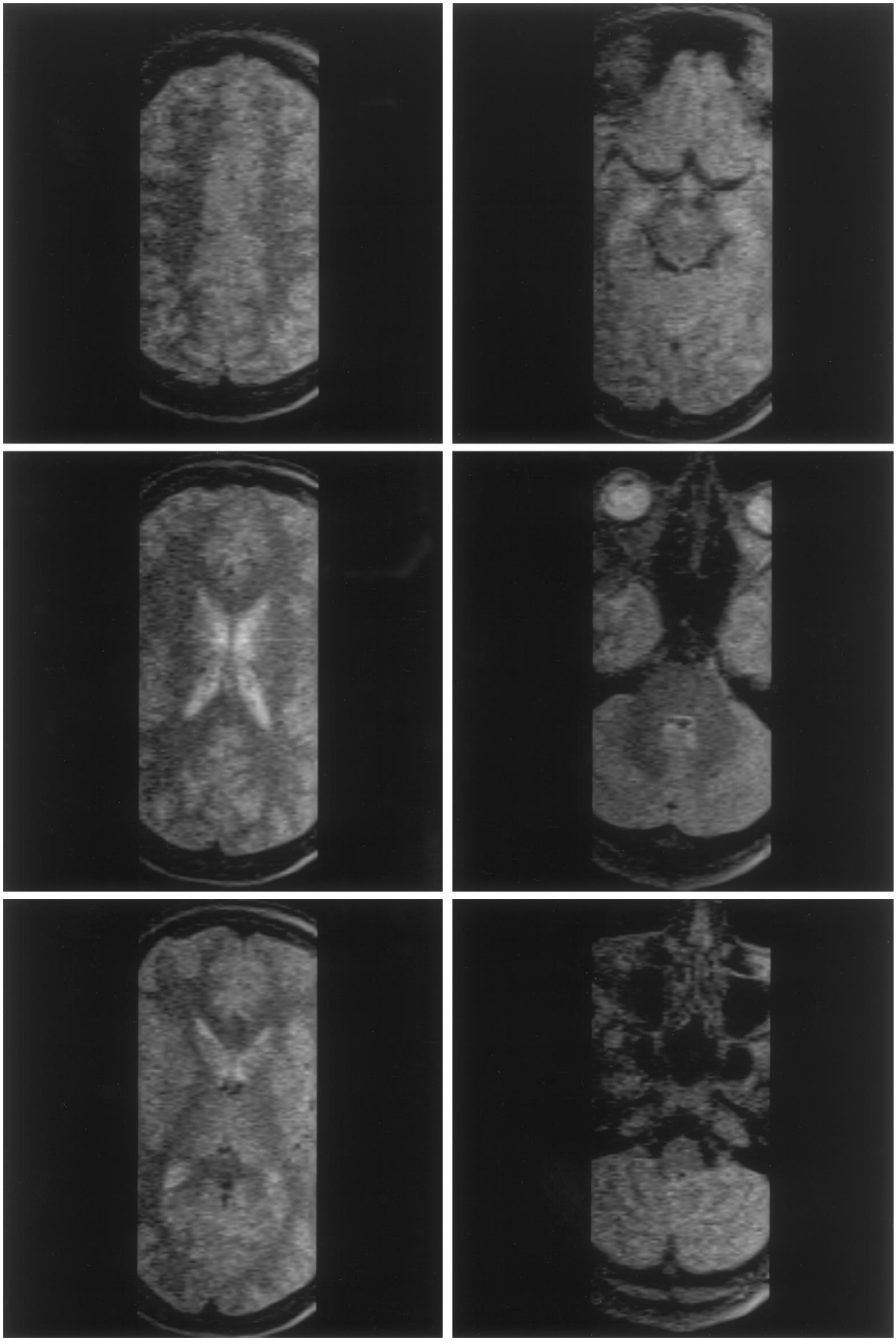

FIG. 5. High-resolution inner volume imaging without aliasing. Sequential acquisitions of single-shot single-slice line scan images of the brain of a healthy young adult (80-mm strip) with a pixel resolution of 1.0×2.0 mm^2 (interpolated to 1.0×1.0 mm^2) and an imaging time of 457 ms (for other parameters see Table 1).

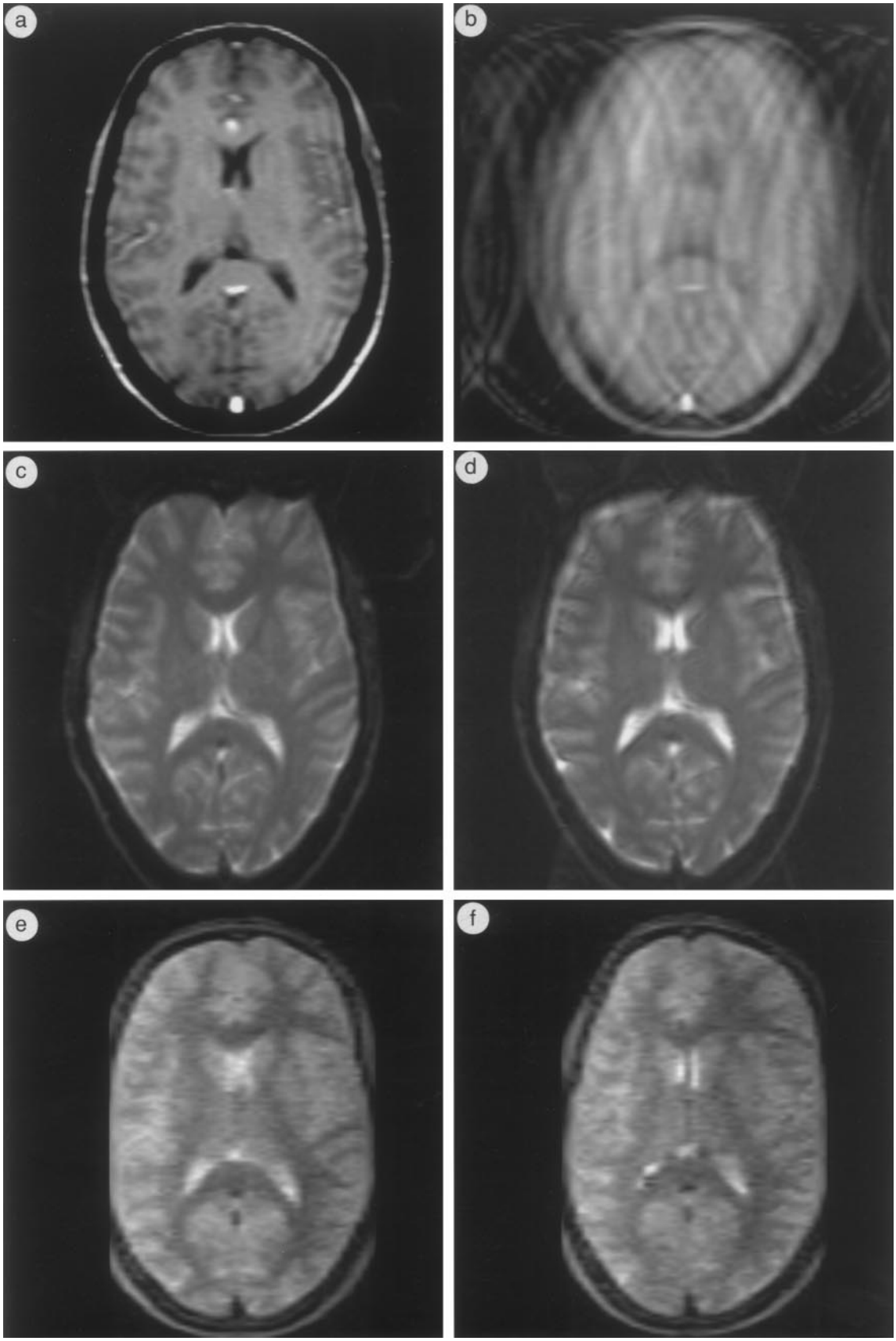

FIG. 6. Motion sensitivity in imaging of the brain of a healthy young adult. (a, b) FLASH images (TR/TE = 45/4 ms, 30° flip angle, 1.5 × 3.0 mm^2, 1/3 sections), (c, d) single-slice SE-EPI (TE = 70 ms, 1.88 × 1.88 mm^2, imaging time 168 ms), and (e, f) single-shot multislice line scan images (1.5 × 3.0 mm^2, 1/3 sections, 443 ms, for other parameters see Table 1) in the absence (left) and presence (right) of shaking head movements.

REFERENCES

1. P. Mansfield, A. A. Maudsley, and T. Baines, *J. Phys. E* **9,** 271–278 (1976).
2. P. Mansfield and A. A. Maudsley, *Brit. J. Radiol.* **50,** 188–194 (1977).
3. P. Mansfield, I. L. Pykett, P. G. Morris, and R. E. Coupland, *Brit. J. Radiol.* **51,** 921–922 (1978).
4. A. A. Maudsley, *J. Magn. Reson.* **41,** 112–126 (1980).
5. L. E. Crooks, *IEEE Trans. Nucl. Sci.* **27,** 1239–1244 (1980).
6. W. A. Edelstein, J. M. Hutchison, G. Johnson, and T. Redpath, *Phys. Med. Biol.* **25,** 751–756 (1980).
7. R. Turner and D. Le Bihan, *in* "Diffusion and Perfusion Magnetic Resonance Imaging" (D. Le Bihan, Ed.), pp. 50–56, Raven, New York (1995).
8. T. A. Case, G. Krishnamurthy, and D. C. Ailion, *in* "Proceedings, SMRM, 6th Scientific Meeting," p. 227 (1987).
9. H. Gudbjartsson, S. E. Maier, R. V. Mulkern, I. Á. Mórocz, S. Patz, and F. A. Jolesz, *Magn. Reson. Med.* **36,** 509–519 (1996).
10. H. Gudbjartsson, S. E. Maier, and F. A. Jolesz, *Magn. Reson. Med.* **38,** 101–109 (1997).
11. D. Jensen and D. Holz, *in* "Proceedings, SMRM, 7th Scientific Meeting, Work in Progress," p. 117 (1988).
12. M. E. Meyerand and E. C. Wong, *Magn. Reson. Med.* **34,** 618–622 (1995).
13. P. Mansfield, *J. Phys. C* **10,** 349–352 (1977).
14. J. Hennig, A. Nauerth, and H. Friedburg, *Magn. Reson. Med.* **3,** 823–833 (1986).
15. Y. Crémillieux, C. A. Wheeler-Kingshott, A. Briguet, and S. J. Doran, *Magn. Reson. Med.* **38,** 645–652 (1997).
16. J. Frahm, A. Haase, D. Matthaei, K.-D. Merboldt, and W. Hänicke, *J. Magn. Reson.* **65,** 130–135 (1985).